Europe PMC Funders Group
Author Manuscript
Nat Struct Mol Biol. Author manuscript; available in PMC 2018 July 22.

Published in final edited form as:
Nat Struct Mol Biol. 2018 February ; 25(2): 147–153. doi:10.1038/s41594-017-0021-5.

TRF1 participates in chromosome end protection by averting TRF2-dependent telomeric R-loops

Yong Woo Lee[1], **Rajika Arora**[1], **Harry Wischnewski**[2], and **Claus M. Azzalin**[1]

[1]Instituto de Medicina Molecular (iMM Lisboa), Faculdade de Medicina da Universidade de Lisboa, Lisbon, 1649-028, Portugal [2]Institute of Biochemistry (IBC), Eidgenössische Technische Hochschule Zürich (ETHZ), Zurich, CH-8093, Switzerland

Abstract

The shelterin protein TRF2 assembles protective T-loops at chromosome ends by stimulating intramolecular invasion of the telomeric G-rich ssDNA overhang into the duplex telomeric array. The other shelterin factor TRF1 is thought to mainly facilitate telomeric dsDNA replication without directly participating in end protection. Here we show that *in vitro* human TRF2 stimulates invasion of G-rich TERRA-like RNA into telomeric dsDNA leading to formation of telomeric RNA:DNA hybrids (telR-loops). The N-terminal basic domain of TRF2 binds to TERRA-like RNA and enables TRF2 to promote efficient RNA invasion. TRF1, through its N-terminal acidic domain, counteracts TRF2-mediated RNA but not ssDNA invasion. *In vivo*, when TRF1 is depleted or replaced with a variant lacking the acidic domain, TRF2 induces formation of telR-loops, which in turn cause telomere loss. Hence, uncontrolled TRF2 threatens telomere integrity and TRF1 directly supports end protection by suppressing harmful telR-loops.

Introduction

Telomeres are nucleoprotein protective structures located at the termini of linear chromosomes. Telomeres comprise three nucleic acid species: double-stranded (ds) DNA repeats (5′-TTAGGG-3′/5′-CCCTAA-3′ in humans), single-stranded (ss) DNA repeats resulting from protrusion of the 3′ G-rich strand over its complement (the G-overhang), and the ss G-rich long noncoding RNA (lncRNA) TERRA1,2. Human TERRA is transcribed by RNA polymerase II from subtelomeric CpG island promoters and contains stretches of the (UUAGGG)n sequence3,4. After transcription, TERRA remains partly associated with telomeric chromatin, and is thus in close proximity to its DNA template3,5.

Users may view, print, copy, and download text and data-mine the content in such documents, for the purposes of academic research, subject always to the full Conditions of use:http://www.nature.com/authors/editorial_policies/license.html#terms

Correspondence should be addressed to C.M.A. (cmazzalin@medicina.ulisboa.pt).

Author Contributions

Y.W.L and C.M.A. conceived and supervised the project; Y.W.L., R.A., H.W. and C.M.A. performed and analyzed the experiments; Y.W.L., R.A. and C.M.A. wrote the manuscript.

Competing Financial Interests

The authors declare no competing financial interests

Europe PMC Funders Author Manuscripts
Europe PMC Funders Author Manuscripts

Europe PMC Funders Author Manuscripts

Europe PMC Funders Author Manuscripts

The multiprotein complex shelterin supports chromosome integrity by preventing inappropriate DNA damage signaling and repair at telomeres6,7. When shelterin is dysfunctional, chromosome ends are sensed as DNA double strand breaks (the end-protection problem) and become substrates for at least one of six DNA damage response pathways, ultimately leading to genome instability6,8. Homodimers of the shelterin DNA-binding proteins TRF1 and TRF2 recognize ds telomeric repeats and recruit the other shelterin components to telomeres6,7. Although the N-terminal sequences of TRF1 (acidic A domain) and TRF2 (basic B domain) are largely divergent, the remaining homodimerization (TRFH), Hinge, and Myb domains are structurally related9. TRF1 is thought to not directly participate in solving the end-protection problem, but rather to assist in semiconservative replication of telomeres, in part by recruiting helicases that resolve secondary structures formed by the G-rich strand10,11. Consistently, TRF1 suppresses activation of the replication stress-associated kinase ATR (ataxia telangiectasia and Rad3 related) and prevents formation of fragile telomeres (FTs), a signature of compromised DNA replication, and, to a lesser extent, of telomere-free chromosome ends (TFEs) of unclear origin10,12. TRF2 suppresses activation of the DNA damage kinase ATM (ataxia telangiectasia mutated) and non-homologous end joining-mediated telomeric fusions13. TRF2 caps chromosome ends largely through its ability to stimulate intramolecular invasion of the G-overhang into the duplex telomeric array thereby forming protective lasso-like structures known as T-loops14,15.

Results

TRF2 stimulates TERRA invasion of ds telomeric DNA *in vitro*

We rationalized that TERRA, like the G-overhang, might invade ds telomeric repeats. We established an *in vitro* invasion assay in which a plasmid containing a telomeric DNA array (p-Tel) is incubated with radiolabeled ss oligonucleotides and then electrophoresed in non-denaturing agarose gels16. Oligonucleotide-invaded plasmids are visualized as slowly migrating bands distinguishable from the free ss oligonucleotides. RNA and DNA oligonucleotides comprising 5 G- or C-rich telomeric repeats readily invaded p-Tel in a sequence-specific manner, as random-sequence oligonucleotides did not invade p-Tel and none of the tested oligonucleotides invaded a control empty plasmid (Supplementary Fig. 1a,b). Treatment of reaction products with recombinant RNaseH, an endonuclease that degrades the RNA moiety of RNA:DNA duplexes, prior to electrophoresis strongly decreased the invaded plasmid signals (Supplementary Fig. 1c). This shows that RNA invasion led to R-loop formation.

We then carried out invasion assays with telomeric RNA and DNA oligonucleotides in the presence of glutathione S-transferase (GST)-tagged recombinant TRF proteins (Supplementary Fig. 2a,b). When incubated with radiolabeled oligonucleotides followed by electrophoresis in denaturing polyacrylamide gels, none of the recombinant proteins utilized in this study affected the radioactive signal (Supplementary Fig. 2c), thus excluding the presence of contaminating RNase, DNase or phosphatase activities. GST-TRF1, GST-TRF2 and GST alone did not alter invasion of C-rich RNA and DNA nor of G-rich DNA at concentrations up to 80 nM (Fig. 1). GST-TRF2, but not GST-TRF1 or GST, stimulated

Europe PMC Funders Author Manuscripts

Europe PMC Funders Author Manuscripts

invasion of G-rich TERRA-like RNA (Figs. 1 and 2a) and R-loop formation (Fig. 2a and Supplementary Fig. 1d) in a concentration-dependent manner. Consistent with published data16,17, GST-TRF2 stimulated G-rich DNA invasion starting at ˜100 nM concentration, where maximum G-rich RNA invasion was already achieved (Fig. 3a). High concentrations of GST-TRF1 had no effect on RNA or DNA invasion (Fig. 3a). A truncated variant of TRF2 lacking the B domain (GST-TRF2ΔB) failed to promote RNA invasion at low concentrations (Fig. 2a; Supplementary Fig. 2a,b), while, at high concentrations, it stimulated RNA and DNA invasion to similar extents although less efficiently than GST-TRF2 (Fig. 3a). A TRF2 variant lacking the C-terminal dsDNA binding Myb domain18 (GST-TRF2ΔM), and another variant unable to induce topological changes in telomeric DNA (GST-Topless)17 did not stimulate RNA or DNA invasion at any of the tested concentrations (Fig. 2a; Supplementary Fig. 2a,b; data not shown). Finally, heat denatured GST-TRF2 also failed to induce RNA invasion (Fig. 2a).

As expected, in electrophoretic mobility shift assays (EMSAs), GST-TRF2ΔM did not bind to telomeric dsDNA substrates while GST-Topless bound similarly to GST-TRF2 (Supplementary Fig. 2d and Supplementary Table 1). GST-TRF2ΔB bound to dsDNA approximately four-fold less efficiently than GST-TRF2 (Supplementary Fig. 2d,e and Table 1), which is not sufficient to explain GST-TRF2ΔB inefficiency in stimulating RNA invasion. In fact, while GST-TRF2 promoted maximum RNA invasion already at ˜40 nM concentrations (Figs. 1 and 2a), GST-TRF2ΔB only induced a ˜1.5 fold increase in RNA invasion at ˜400 nM concentrations (Fig. 3a). We conclude that TRF2 stimulates G-rich RNA invasion with higher efficiencies than it does with G-rich DNA. This novel TRF2-associated activity requires TRF2 binding to and wrapping of ds telomeric DNA, as is also the case for G-rich DNA invasion16,17, and is specifically potentiated by TRF2 B domain. Further reinforcing the importance of the B domain for efficient RNA invasion, a chimeric protein where the A domain of TRF1 was swapped with the B domain of TRF2 (GST-BTRF1ΔA) readily induced RNA invasion (Supplementary Figs. 2a,b and 3a), despite binding to telomeric dsDNA ˜18 fold less efficiently than GST-TRF2 (Supplementary Fig. 2e and Supplementary Table 1).

TRF1 A domain suppresses TRF2-stimulated TERRA invasion of ds telomeric DNA *in vitro*

We next performed G-rich RNA invasion reactions with fixed amounts of GST-TRF2 combined with increasing amounts of GST-TRF1, and observed a progressive decline in invaded plasmid species (Figs. 2b and 3b). In contrast, GST-TRF1 did not inhibit the G-rich DNA invasion stimulated by high concentrations of GST-TRF2 (Fig. 3b). A truncated variant of TRF1 lacking the A domain (GST-TRF1ΔA) failed to neutralize GST-TRF2-stimulated RNA invasion at any of the tested concentrations (Figs. 2b and 3b; Supplementary Fig. 2a,b). As with GST-TRF1, GST-TRF1ΔA did not promote RNA invasion (Supplementary Fig. 3a) nor did it prevent GST-TRF2 from inducing DNA invasion at high concentrations (Fig. 3b). Because the Myb domains of TRF1 and TRF2 bind the same dsDNA substrate18, we considered the possibility that GST-TRF1 counteracted GST-TRF2 by diminishing its density on DNA and GST-TRF1ΔA simply binds dsDNA substantially less efficiently than its full-length counterpart. However, GST-TRF1ΔA bound only ˜1.1-to-1.5 fold less efficiently than GST-TRF1 to telomeric dsDNA substrates

Europe PMC Funders Author Manuscripts

Europe PMC Funders Author Manuscripts

(Supplementary Fig. 2d,e and Supplementary Table 1). These minor differences are unlikely to explain why GST-TRF1ΔA did not suppress TRF2-mediated RNA invasion, as the chosen concentration ranges for TRF1 proteins covered a very wide range going from 0 to 400 nM (Figs. 2b and 3b).

Additional evidence argues against the hypothesis that GST-TRF1 suppresses GST-TRF2-mediated RNA invasion through dsDNA substrate competition. First, in dsDNA EMSAs with increasing amounts of GST-TRF1 or GST-TRF1ΔA in presence or absence of fixed amounts of GST-TRF2, bound probes further shifted towards the wells when GST-TRF2 was included (Supplementary Fig. 3b); this indicates that GST-TRF1/TRF1ΔA and GST-TRF2 concomitantly bound to the same substrate in our experimental conditions. Second, western blotting analysis of strand invasion products revealed no change in the amounts of dsDNA-bound GST-TRF2 when GST-TRF1/TRF1ΔA were included in the reactions (Supplementary Fig. 3c). We also considered the possibility that the apparent inability of GST-TRF1ΔA to inhibit GST-TRF2 stimulated RNA invasion rather derived from a putative ability of GST-TRF1ΔA but not of GST-TRF1 to bind and thus stabilize telomeric RNA:DNA hybrids. However, none of the recombinant TRF proteins used in this study bound to telomeric RNA:DNA hybrid substrates, contrarily to GST fused to the hybrid binding domain of human RNaseH119 (Supplementary Figs. 2a,b and 3d). We conclude that TRF1 inhibits TRF2-stimulated invasion of TERRA, but not of G-rich ssDNA, and this inhibitory activity requires the A domain.

TRF1 A domain suppresses the ability of TRF2 B domain to bind to TERRA in vitro

To shed some light on the mechanisms through which the A domain suppresses TRF2-stimulated RNA invasion, we set up RNA EMSAs and found that, consistent with previously published data20, GST-TRF2, GST-TRF2ΔB, GST-TRF1 and GST-TRF1ΔA bound to G-rich telomeric RNA oligonucleotides but not to C-rich or random sequence RNA oligonucleotides nor to telomeric or random sequence DNA oligonucleotides (Fig. 4a,b and Supplementary Fig. 3e). TRF2ΔB bound to G-rich RNA less efficiently than GST-TRF2, while GST-TRF1 and GST-TRF1ΔA binding kinetics were indistinguishable (Fig. 4a,b and Supplementary Table 1). Consistently, GST fused to the B domain (GST-B) bound to G-rich RNA, while GST fused to the A domain (GST-A) did not (Fig. 4a,b; Supplementary Fig. 2a,b and Supplementary Table 1). Fusing the A domain to the N-terminus of the B domain (GST-AB) largely abolished RNA binding, while fusing the A domain to the N-terminus of TRF2 (GST-ATRF2) decreased binding to efficiencies comparable to that of GST-TRF2ΔB (Fig. 4a,b; Supplementary Fig. 2a,b and Supplementary Table 1). As expected, GST-A, GST-B and GST-AB did not bind to telomeric dsDNA (Supplementary Fig. 2f).

Based on these experiments, we propose that the direct binding of G-rich RNA to the B domain drives the highly efficient TRF2-stimulated RNA invasion, and that the A domain of TRF1 counteracts this mechanism most likely by impeding the interaction between the B domain and G-rich RNA. Consistent with this hypothesis, at low concentrations, GST-ATRF2 failed to promote efficient RNA invasion although its ability to bind to telomeric dsDNA was not compromised (Fig. 4c; Supplementary Fig. 2d and Supplementary Table 1).

Europe PMC Funders Author Manuscripts

Europe PMC Funders Author Manuscripts

Similar to GST-TRF2ΔB, GST-ATRF2 mildly stimulated RNA and DNA invasion at high protein concentrations (Fig. 3a).

TRF1 A domain suppresses telR-loops in cells

Our *in vitro* data suggest that TRF1 and TRF2 crosstalk to regulate TERRA interaction with telomeric dsDNA in cells. We depleted TRF1 using short interference RNAs (siRNAs) in telomerase-positive HeLa and ALT (Alternative Lengthening of Telomeres21) U2OS cancer cells, and quantified telR-loops by immunoprecipitation with the RNA:DNA hybrid-specific S9.6 antibody (S9.6 DRIPs), followed by dot-blot hybridization22,23. In both cell lines, TRF1 depletion increased telR-loops but not R-loops containing Alu repeat sequences (Fig. 5a; Supplementary Figs. 4a,b and 5a-c). Ectopic expression of siRNA-insensitive, flag-tagged TRF1 (fl-TRF1) in TRF1-depleted HeLa cells prevented telR-loop accumulation, while an A-deleted counterpart (fl-ΔA) did not (Fig. 5b; Supplementary Fig. 4a,b). In fact, fl-ΔA expression alone increased telR-loops (Fig. 5b; Supplementary Figs. 4b), suggesting a dominant-negative effect likely through replacement of endogenous TRF1 at telomeres (Supplementary Fig. 6a-c). Notably, combining TRF1 depletion with fl-ΔA expression did not significantly increase telR-loops above single conditions (Fig. 5b), indicating impairment of the same TRF1-associated function in suppressing telR-loops. The TRF1 A domain recruits the poly(ADP-ribose) polymerase Tankyrase 1 (TNK1) to telomeres24. We siRNA-depleted TNK1 in HeLa and U2OS cells and observed the expected accumulation of mitotic cells25 (Supplementary Fig. 7a,b). However, TNK1 depletion did not alter telR-loop levels (Supplementary Fig. 7c), excluding that the increased telR-loops in cells depleted of TRF1 or expressing fl-ΔA results from insufficient TNK1 at telomeres.

TRF1 A domain suppresses R-loop-dependent telomere instability

In ALT cells, aberrant accumulation of telR-loops leads to telomere dysfunction-induced foci (TIFs) containing telomeric DNA and a serine 33-phosphorylated form of the ssDNA binding protein RPA32 (pSer33), and to metaphase TFEs22. pSer33 also accumulates at R-loops throughout the genome26. TRF1 depletion and fl-ΔA expression increased pSer33 TIFs and TFEs both in HeLa (Figs. 5c,d and 6a,b; Supplementary Fig. 4c,d) and U2OS (Fig. 7a,b and Supplementary Fig. 5d) cells. TFEs were detected at chromosome ends generated by both lagging and leading strand replication (Figs. 6a,b and 7a,b). fl-TRF1, but not fl-ΔA, prevented accumulation of pSer33 TIFs and TFEs in cells depleted of endogenous TRF1 (Figs. 5c,d and 6a,b; Supplementary Fig. 4c,d). As expected10, FTs also accumulated in TRF1 depleted cells (Fig. 6a,b and 7a; Supplementary Fig. 4d); both fl-TRF1 and fl-ΔA averted the increase in FTs in the same cells (Fig. 6a,b and Supplementary Fig. 4d), and suppressed spontaneous FTs in cells where endogenous TRF1 was not depleted (Figs. 6b and 7b).

Ectopic expression of a myc-tagged version of the human RNaseH1 endoribonuclease ($RH1^{wt}$) prevented accumulation of telR-loops, pSer33 TIFs and TFEs upon TRF1 depletion or fl-ΔA expression, while a catalytically dead RNaseH1 ($RH1^{CD}$)19 did not (Figs. 5b,d and 6b; Supplementary Fig. 4a,b,e-l). FTs accumulated at similar frequencies in TRF1 depleted cells expressing either $RH1^{wt}$ or $RH1^{CD}$ (Fig. 6b). These data establish that suppression of pSer33 TIFs and TFEs through restriction of telR-loops are previously unappreciated TRF1

functions that strictly depend on the A domain and are genetically separable from fragility suppression.

TelR-loops suppressed by TRF1 A domain depend on TRF2

Our biochemical data suggest that TRF1 A domain suppresses telR-loops induced by TRF2-stimulated TERRA invasion. To test this hypothesis in cells, we first over-expressed N-terminally myc-tagged TRF2 (m-TRF2) and ATRF2 (m-ATRF2) in HeLa cells and found that m-TRF2 but not m-ATRF2 increased telR-loop and pSer33 TIF levels (Fig. 8 a-e). This might explain the stochastic telomere loss and consequent TFE appearance observed in human and mouse cells overexpressing TRF227,28. Furthermore, depleting endogenous TRF2 prevented accumulation of telR-loops in TRF1-depleted (Supplementary Fig. 8a,b) and in fl-ΔA-expressing (Supplementary Fig. 8c,d) cells. Consistent with the notion that uncontrolled TRF2-dependent telR-loops cause telomere instability, TRF2 depletion averted the insurgence of pSer33 TIFs and TFEs in fl-ΔA-expressing cells (Fig. 5d; Supplementary Fig. 8e,f). As expected, TRF2 depletion did not affect FT frequencies (Supplementary Fig. 8f).

Discussion

We have identified two novel, interdependent activities at human telomeres: *i*) TRF2 promotes TERRA invasion into telomeric dsDNA likely through the ability of the B domain to directly interact with TERRA possibly recruiting it to telomeres, and through the ability of the TRFH domain to wrap telomeric dsDNA and alter its topology; *ii*) TRF1, through its A domain, maintains constant control of this TERRA invasion activity dependent on TRF2 (Fig. 8f). The molecular basis of how TRF1 discriminates RNA from DNA during TRF2-mediated strand invasion remains to be determined. Still, because TRF2 B domain is only able to interact with TERRA and not with telomeric ssDNA, this discrimination probably derives from TRF1 A domain ability to prevent TERRA from interacting with TRF2 B domain. We have also shown that in the absence of controlled crosstalk between these novel activities (a situation recapitulated by TRF1 depletion or TRF1ΔA expression in cells), aberrant telR-loops accumulate and lead to pSer33 TIFs and telomere loss (Fig. 8f). We therefore propose that uncontrolled TRF2 and telR-loops pose authentic threats to telomere integrity, and that TRF1 directly contributes to solving the end-protection problem by suppressing unscheduled telR-loop-induced telomere instability.

Our data unambiguously demonstrate the harmful potential of TRF2-dependent telR-loops, thus questioning the evolutionary and functional advantage of this unexpected TRF2 activity. One possibility is that TERRA invasion is a secondary, unwanted reaction associated to TRF2-mediated stimulation of T-loop formation. In this light, the A domain might have evolved to specifically prevent telR-loop formation without interfering with T-loop establishment. However, disfavoring this simple hypothesis, our *in vitro* data suggest that TRF2 stimulates TERRA invasion with higher efficiency than G-overhang invasion. It is possible that programmed TRF2-mediated RNA invasion, promoted by regulated TRF1 removal from telomeres29 for example, may serve specific functions in certain cellular settings, such as during replicative senescence, telomerase recruitment and telomere

Europe PMC Funders Author Manuscripts
Europe PMC Funders Author Manuscripts

Europe PMC Funders Author Manuscripts

Europe PMC Funders Author Manuscripts

recombination22,29–31. Moreover, TRF2 B domain was shown to bind to three- and four-way Holiday junctions irrespective of their sequences and such activity was recently proved essential to prevent T-loop cleavage and telomere excision32–34. It will be important to determine to what extent the functions of the B domain in promoting TERRA invasion and repressing T-loop cleavage are interconnected. Lastly, RNA-invasion activities like that of TRF2 could be involved in the formation of intrachromosomal, post-transcriptional R-loops comprising messenger or noncoding RNAs of non telomeric origin. Because genome wide spread R-loops are well-established triggers of chromosome instabilities that are frequently observed in cancer cells35, the identification of such activities could help deepen our understanding of cancer etiology.

Online Methods

Plasmids

TRF1 and TRF2 cDNAs were derived from the pLPC-NFLAGTRF1 and pLPC-NMYCTRF2 retroviral vectors (kind gifts from Titia de Lange). TOPLESS cDNA was a kind gift for Eric Gilson. All successive manipulations were performed by PCR and validated by sequencing. For expression in mammalian cells, we deleted the A domain sequence from the pLPC-NFLAGTRF1 plasmid or cloned both NFLAGTRF1 and NFLAGTRF1ΔA cDNAs into the lentiviral vector pLVX-TetOne-Puro (Clontech). NMYCTRF2 and NMYCATRF2 cDNAs were cloned into the pLVX-TetOne-Puro vector. Full-length human RNASEH1 cDNA was purchased from Origene, fused in frame with a C-terminal Myc tag and cloned into the retroviral vector pLHCX (Clontech). Catalytically dead RNASEH1 was obtained by changing the aspartic acid at position 145 into alanine (D145A)19 using the Q5 site directed mutagenesis kit (New England Biolabs). For expression in bacteria cells, cDNAs for different TRF proteins were N-terminally fused in frame to a GST sequence by cloning into the pGEX-4T1 vector (GE Healthcare). The RNA:DNA hybrid binding domain of RNaseH1 was PCR amplified from the pLHCX-MYCRNASEH1 plasmid and cloned into the pGEX-4T1 vector. The p-Tel plasmid was generated by cloning a stretch of ~800 bp of telomeric DNA (kind gift from Eric Gilson) into pcDNA6 (Life Technologies).

Cell lines and tissue culture procedures

HeLa telomerase positive cervical cancer cells (ATCC) and U2OS osteosarcoma cells (kind gift from Joachim Lingner) were cultured in high glucose D-MEM (Invitrogen) supplemented with 10% TET-free fetal bovine serum (Pan BioTech) and penicillin/streptomycin (Sigma-Aldrich). The two cell lines are not listed as commonly misidentified (NCBI Biosample) and they tested negative for mycoplasma contamination using the VenorGeM Mycoplasma PCR Detection Kit (Minerva Biolabs). Virus infections were performed according to standard procedures followed by selection with 1.5 μg/ml puromycin (Sigma-Aldrich) for pLPC- and pLVX-TetOne-Puro-derived viruses or with 200 μg/ml hygromycin (Invitrogen) for pLHCX-derived viruses. For cells infected with pLVX-TetOne-Puro lentiviruses, protein expression was induced with 0.5 μg/ml doxycycline (Sigma-Aldrich). siRNAs were purchased from Integrated DNA Technologies and transfected using the Lipofectamine RNAiMAX reagent (Invitrogen) at 20-25 nM concentrations. Sequences

Europe PMC Funders Author Manuscripts

Europe PMC Funders Author Manuscripts

were: siCt (control): 5'-AUACGCGUAUUAUACGCGAUUAAC-3'; siT1c (TRF1): 5'-CUUUCUUUCUUAUUAAGGUCUUGUUGC-3'; siT1e (TRF1 5' UTR): 5'-CGAGCCAUUUAACAUGGCGGAGGAU-3'; siT2 (TRF2): 5'-AGAAUCCCAAAGUACCCAAAGGCAA-3'; siTNK1 (Tankyrase 1): 5'-GGCUACAACAGACUUCGAAUAGU-3'

Western blotting

Total proteins prepared in 2X Laemmli buffer were separated in 8-10% polyacrylamide gels and transferred to nitrocellulose membranes (Maine Manufacturing LLC) using a Trans-Blot SD Semi-Dry Transfer Cell apparatus (Bio-Rad). Western blots were performed according to standard procedures using the following primary antibodies: a mouse monoclonal anti-TRF2 (Millipore, 05-521, dilution 1:2000), a rabbit polyclonal anti-TRF1 raised against full-length recombinant TRF1 (kind gift from Jan Karlseder, 1:2000), a rabbit polyclonal anti-Tankyrase 1 (kind gift from Susan Smith, 1:5000), a rabbit polyclonal anti-RNaseH1 (GeneTex, GTX117624, 1:1000), a mouse monoclonal anti-hbetaActin (Abcam, ab8224, 1:10000), and a rabbit polyclonal anti-LaminA (GeneTex, GTX111677S, 1:5000). Secondary antibodies were HRP-conjugated goat anti-mouse and anti-rabbit IgGs (Bethyl Laboratories, 1:5000). Signals were acquired using a FluorChem HD2 apparatus (Alpha Innotech).

DNA FISH and CO-FISH

Metaphase DNA FISH was performed as previously described3. Briefly, cells were treated with 200 ng/ml Colcemid (Sigma-Aldrich) for 2-3 hours, harvested and incubated in 0.075 M KCl for 9 min at 37 °C. Chromosomes were fixed in cold methanol/acetic acid (3:1), spread on glass slides and treated with 20 μg/ml DNase-free RNaseA (Sigma-Aldrich), 1X PBS for 1 hour at 37 °C. Hybridizations were performed in 30% formamide, 2X SSC for 3 hours at room temperature with a TexasRed-labeled LNA probe (5'-Tex615-GGGT*TAGGG*T*TAG*GGTTAGGG*T*TAGGG*T*TAGGG*TTA-3'; asterisks indicate LNA nucleotides; Exiqon). Post-hybridization washes were in 2X SSC at room temperature. DNA was counterstained with DAPI (Sigma-Aldrich). Metaphase CO-FISH was performed as previously described8 with some modifications. Cells were incubated with BrdU:BrdC (3:1, final concentration 10 μM) for 16 hours prior to metaphase preparation as above. Chromosomes were spread on glass slides, treated with DNase-free RNaseA as above and incubated with 10 μg/ml Hoechst 33258 (Invitrogen) in 2X SSC for 15 min at room temperature. Slides were then exposed to 365-nm ultraviolet light using a Stratagene Stratalinker 1800 UV irradiator set to 5400 Joules, and incubated with 3U/μl Exonuclease III (New England Biolabs) for 30 min at 37 °C. Hybridizations were performed in 30% formamide, 2X SSC for 3h at room temperature using 6-FAM- or TYE563-labeled LNA probes (TelC LNA probe: 5'-6-FAM-CCC*TAACCC*TAACCC*TAA-3'; TelG LNA probe: 5'-TYE563-T*TAGGGT*TAGGGT*TAGGG; asterisks indicate LNA nucleotides; Exiqon). Post-hybridization washes were in 2X SSC at room temperature. DNA was counterstained with DAPI (Sigma-Aldrich). Images were acquired with an Olympus IX 81 microscope equipped with a Hamamatsu ORCA-ER camera using a 60X 1.42NA oil PlanAPoN objective, or with a Deltavision Multiplexed system (Applied Precision) with an Olympus 1X 71 (inverse) microscope, Roper CoolSnap HQ2 camera and a 60X 1.4NA oil DIC

Europe PMC Funders Author Manuscripts

Europe PMC Funders Author Manuscripts

PlanAPoN objective. Images were analyzed using ImageJ and Adobe Photoshop. Statistical analysis was performed in Prism (GraphPad) with a Mann-Whitney *U* test as indicated in figure legends. The number of independent experiments (*n*) is also indicated in figure legends.

Indirect immunofluorescence

Cells grown on coverslips were washed with ice-cold 1X PBS and soluble cellular material was extracted with CSK buffer (100 mM NaCl, 300 mM sucrose, 3 mM $MgCl_2$, 0.5% Triton X-100, 10 mM PIPES pH 6.8) for 7 min on ice. Cells were fixed in 3.7% formaldehyde for 10 min, washed in 1X PBS and permeabilized again with CSK buffer for 5 min at room temperature. Cells were blocked in 5 mg/ml BSA, 0.05% Tween-20 in 1X PBS, and then incubated with primary antibodies diluted in blocking solution for 1 h at room temperature. Antibodies were as follows: a mouse monoclonal anti-Flag (Sigma-Aldrich, F1804, 1:1000), a mouse monoclonal anti-Myc (Sigma-Aldrich M4439, 1:500), a rabbit polyclonal anti-pSer33, (Bethyl Laboratories A300-244A, 1:500), a mouse monoclonal anti-TRF2 (Millipore, 05-521, 1:500), and a mouse monoclonal mix raised against a recombinant peptide spanning the A domain of hTRF1 (raised at the monoclonal antibody facility of Max F. Perutz Laboratories in Vienna, 1:100). Secondary antibodies were donkey anti-rabbit and donkey anti-mouse IgGs conjugated with Alexa Fluor 568 or Alexa Fluor 488 (Invitrogen, 1:5000). For IF/DNA FISH, immunostained cells were fixed with 3.7% formaldehyde for 10 min at room temperature and hybridized as for metaphase DNA FISH. Images were acquired with an Olympus IX 81 microscope equipped with a Hamamatsu ORCA-ER camera using a 60X 1.42NA oil PlanAPoN objective or the Zeiss Cell Observer equipped with a cooled Axiocam 506m camera and using a 63x/1.4NA oil DIC M27 PlanApo objective. 20 z sections of 0.5 μm were taken and co-localization analysis was performed using ImageJ on separate sections. A total of 100 nuclei were analyzed for each sample in each independent experiment. Statistical analysis was performed in Microsoft Excel using a two-tailed Student's *t*-test as indicated in figure legends. The number of independent experiments (*n*) is also indicated in figure legends.

GST protein purification

The pGEX-4T1 plasmids were transformed into competent BL21 cells. Cells were grown in LB media until they reached an O.D of 0.4 (600 nm) and protein expression was induced with 50 μM IPTG (Sigma-Aldrich) for 5 hours at 25 °C. Cells were collected by centrifugation and lysed by sonication in 25 ml of GST pull-down buffer (50 mM potassium phosphate buffer pH 7, 5 mM EDTA, 100 mM NaCl, 1% Triton X-100, 0.15 mM PMSF). Lysates were incubated with Glutathione Sepharose 4B beads (GE Healthcare) in GST pull-down buffer for 5 hours at 4 °C on a rotating wheel. Beads were washed with 10 ml of GST pull-down buffer 3 times and bound proteins were eluted in 200 μl of GST elution buffer (50 mM potassium phosphate buffer pH 7, 5 mM EDTA, 100 mM NaCl, 5% glycerol, 25 mM glutathione) for 15 min at 4 °C. Protein concentration and purity were determined using the Bradford protein assay (Bio-Rad) and BSA reference samples, followed by fractionation of equal amounts of proteins in polyacrylamide gels and staining with the EZBlue reagent (Sigma-Aldrich). Note that all protein concentrations refer to TRF monomers. Proteins were stored at -20 °C for up to one month.

Europe PMC Funders Author Manuscripts

Europe PMC Funders Author Manuscripts

Strand invasion assays

Strand invasion assays were performed adapting previously described protocols16,36. pcDNA6 and p-Tel plasmids were purified using the GeneJET plasmid miniprep Kit (Thermo Fisher Scientific) and re-purified twice using the DNA Clean & Concentrator Kit (Zymo Research) to assure removal of RNase contaminations. DNA and RNA oligonucleotides were synthesized and PAGE purified at Microsynth. Sequences were as follow: 5'-$(TTAGGG)_5$-3', 5'-$(UUAGGG)_5$-3', 5'-$(CCCTAA)_5$-3', 5'-$(CCCUAA)_5$-3', 5'-TATCGATAAGCTTGATATCGAATTCCTGCA-3' (random DNA sequence), and 5'-AGAGAUUGCCUGACGUCAGAGAGCUAGCGA-3' (random RNA sequence). Oligonucleotides were 5'-end labeled with T4 polynucleotide kinase (New England Biolabs) and γ^{32}P-ATP followed by purification using the Oligo Clean & Concentrator Kit (Zymo Research). 50 ng of plasmid (0.6 nM final concentration) were incubated in 20 μl of strand invasion buffer (50 mM HEPES pH 8, 1 mM DTT, 100 mM NaCl, 0.01% BSA, 2% glycerol) containing 10 U of RNaseOUT (Thermo Fisher Scientific) for 20 min at 24 °C in presence or absence of recombinant proteins. Labeled oligonucleotides were then added to the reactions at 10 nM concentrations unless otherwise indicated and incubated for 30 min at 24 °C. When specified, 10 U of RNaseH (New England Biolabs) were added to the reactions followed by an incubation of 15 min at 37 °C. Reactions were stopped by adding 4 μl of 6X gel-loading buffer (30% glycerol, 0.3% bromophenol blue, 0.3% xylene cyanol) containing 12% SDS and incubating for 5 min at room temperature. Reaction products were fractionated by electrophoresis in 1% agarose gels. Gels were dried and exposed to a phosphoimager screen. Radioactive signals were detected using a Typhoon FLA 9000 imager (GE Healthcare) and quantified using ImageJ. Statistical analysis was performed in Microsoft Excel using a two-tailed Student's *t*-test as indicated in figure legends. The number of independent experiments (*n*) is also indicated in figure legends.

Western blotting-strand invasion assays

Reactions were performed exactly as for invasion assays using 50 ng of pTel plasmid (0.6 nM final concentration), the indicated amounts of recombinant proteins and 10 nM 5'-$(UUAGGG)_5$-3' oligonucleotides. Reactions were stopped by adding 4 μl of 6X gel-loading buffer (30% glycerol, 0.3% bromophenol blue, 0.3% xylene cyanol). Products were fractionated by electrophoresis in 1% agarose gels followed by incubation in SDS PAGE running buffer (25 mM Tris-Cl, 192 mM glycine, 0.1% SDS) for 5 min at room temperature and transfer to nitrocellulose membranes (Maine Manufacturing LLC) using a Trans-Blot SD Semi-Dry Transfer Cell apparatus (Bio-Rad). Western blots were performed as above. Signals were acquired using a FluorChem HD2 apparatus (Alpha Innotech) and quantified using ImageJ. Statistical analysis was performed in Microsoft Excel. The number of independent experiments (*n*) is indicated in figure legends.

Electrophoretic mobility shift assay

For ssDNA and RNA EMSAs, oligonucleotides were as for invasion assays. For dsDNA EMSAs, the ds[TTAGGG]24 fragment was PCR amplified from a plasmid gene synthesized at GenScript and contained 24 telomeric repeats flanked by non telomeric sequences of 31 (upstream) and 46 bp (downstream); the ds[TTAGGG]0.8 kb fragment was excised by

Europe PMC Funders Author Manuscripts

Europe PMC Funders Author Manuscripts

restriction digestion from the p-Tel plasmid and contained approximately 800 bp of (TTAGGG)n sequence flanked by non telomeric sequences of 48 (upstream) and 12 bp (downstream). dsDNA fragments were 5'-end labeled with T4 polynucleotide kinase (New England Biolabs) and γ^{32}P-ATP followed by purification using the DNA Clean & Concentrator Kit (Zymo Research). For duplex RNA:DNA EMSAs, the hybrid [UUAGGG:CCCTAA]5 substrate was generated by annealing 5'-end radiolabeled 5'-$(UUAGGG)_5$-3' oligonucleotides with a 2 fold molar excess of unlabeled 5'-$(CCCTAA)_5$-3' oligonucleotides. Recombinant proteins and nucleic acids were incubated in 20 μl of strand invasion buffer containing 50 ng/μl *E. coli* tRNAs (Sigma-Aldrich) and 10 U of RNaseOUT (Thermo Fisher Scientific) for 20 min at 24 °C. 4 μl of 6X gel-loading buffer were added to the reactions followed by electrophoresis in 2% agarose gels. Gels were dried and exposed to a phosphoimager screen. Radioactive signal detection and analysis were as for invasion assays. The number of independent experiments (*n*) is indicated in figure legends.

S9.6 DRIP assays

Cells were harvested by scraping and lysed in 1 ml of RA1 buffer (Macherey-Nagel) containing 1% v/v β-Mercaptoethanol and 100 mM NaCl. Nucleic acids were extracted with phenol:chloroform:isoamyl alcohol (25:24:1 saturated with 10 mM Tris-Cl pH 8.0, 1 mM EDTA), followed by isopropanol precipitation and centrifugation at 14,000 rpm for 10 min at 4 °C. Pellets were washed in 70% ethanol, resuspended in 200 μl Tris-EDTA, 100 mM NaCl, and sonicated using a Bioruptor apparatus (Diagenode). 5 μg of nucleic acids were incubated with 1 μg of mouse monoclonal S9.6 antibody (kind gift from Stephen Leppla) in IP buffer (0.1% SDS, 1% Triton X-100, 10 mM HEPES pH 7.2, 0.1% sodium deoxycholate, 275 mM NaCl) for 5 hours at 4 °C. Immunocomplexes were isolated by incubation with protein G sepharose beads (GE Healthcare) blocked with sheared *E. coli* DNA and BSA. Beads were washed 4 times in IP buffer and incubated in elution buffer (1% SDS, 100 mM $NaHCO_3$) containing 40 μg/ml RNase A (Roche) for 1 hour at 37 °C. DNA was extracted using the Wizard SV gel and PCR cleanup system (Promega), dot-blotted on nylon membranes and hybridized over night at 55 °C with a synthetic telomeric probe random primer labeled with α^{32}P-dCTP. Post-hybridization washes were in 0.2X SSC, 0.2% SDS at 55 °C. After signal detection, membranes were stripped and re-hybridized at 55 °C with Alu repeat oligonucleotides (5'-GTGATCCGCCCGCCTCGGCCTCCCAAAGTG-3') 5'-end labeled with T4 polynucleotide kinase (New England Biolabs) and γ^{32}P-ATP. Post-hybridization washes were in 2X SSC, 0.5% SDS and 0.5X SSC, 0.5% SDS at 55 °C. Radioactive signal detection and analysis were as for invasion assays. The number of independent experiments (*n*) is indicated in figure legends.

Statistical methods

The two-tailed Student's *t*-test was performed using Microsoft Excel to assess statistically significant differences for DRIP and pSer33 TIF analyses. The nonparametric two-tailed Mann-Whitney *U* test was performed using GraphPad Prism to assess significant differences in TFEs and FTs for FISH and CO-FISH analyses. Probability (*P*) values are: $*P < 0.05$, $**P < 0.005$, $***P < 0.0001$. Error bars represent standard deviations (SD).

Europe PMC Funders Author Manuscripts

Europe PMC Funders Author Manuscripts

Data availability

Primary data are available upon request. A Life Sciences Reporting Summary for this article is available.

Supplementary Material

Refer to Web version on PubMed Central for supplementary material.

Acknowledgments

We thank T. de Lange, J. Karlseder, E. Gilson, S. Smith, S. Leppla, and J. Lingner for reagents; the Bioimaging facility of iMM Lisboa and the Scientific Center for Optical and Electron Microscopy of ETHZ for microscopy services; members of the Azzalin laboratory for discussions; and J. Lingner for critical reading of the manuscript. This work was initiated at the Institute of Biochemistry of ETH Zürich and supported by grants awarded to CMA by the Swiss National Science Foundation (31003A_160338), the European Research Council (BFTERRA), EMBO (IG3576) and Fundação para a Ciência e a Tecnologia (IF/01269/2015). YWL was supported by an EMBO long-term fellowship (ALTF 395-2014) and the National Research Foundation of Korea (NRF-2013R1A6A3A03063846). Publication costs were supported through LISBOA-01-0145-FEDER-007391, projeto cofinanciado pelo FEDER através POR Lisboa 2020 - Programa Operacional Regional de Lisboa, do PORTUGAL 2020, e pela Fundação para a Ciência e a Tecnologia.

References

1. Martinez P, Blasco MA. Replicating through telomeres: a means to an end. Trends in Biochemical Sciences. 2015; 40:504–515. [PubMed: 26188776]
2. Azzalin CM, Lingner J. Telomere functions grounding on TERRA firma. Trends Cell Biol. 2015; 25:29–36. [PubMed: 25257515]
3. Azzalin CM, Reichenbach P, Khoriauli L, Giulotto E, Lingner J. Telomeric repeat containing RNA and RNA surveillance factors at mammalian chromosome ends. Science. 2007; 318:798–801. [PubMed: 17916692]
4. Nergadze SG, et al. CpG-island promoters drive transcription of human telomeres. RNA. 2009; 15:2186–94. [PubMed: 19850908]
5. Schoeftner S, Blasco MA. Developmentally regulated transcription of mammalian telomeres by DNA-dependent RNA polymerase II. Nat Cell Biol. 2008; 10:228–36. [PubMed: 18157120]
6. Arnoult N, Karlseder J. Complex interactions between the DNA-damage response and mammalian telomeres. Nat Struct Mol Biol. 2015; 22:859–66. [PubMed: 26581520]
7. de Lange T. How shelterin solves the telomere end-protection problem. Cold Spring Harb Symp Quant Biol. 2010; 75:167–77. [PubMed: 21209389]
8. Sfeir A, de Lange T. Removal of Shelterin Reveals the Telomere End-Protection Problem. Science. 2012; 336:593–597. [PubMed: 22556254]
9. Broccoli D, Smogorzewska A, Chong L, deLange T. Human telomeres contain two distinct Myb-related proteins, TRF1 and TRF2. Nat Genet. 1997; 17:231–235. [PubMed: 9326950]
10. Sfeir A, et al. Mammalian telomeres resemble fragile sites and require TRF1 for efficient replication. Cell. 2009; 138:90–103. [PubMed: 19596237]
11. Zimmermann M, Kibe T, Kabir S, de Lange T. TRF1 negotiates TTAGGG repeat-associated replication problems by recruiting the BLM helicase and the TPP1/POT1 repressor of ATR signaling. Genes Dev. 2014; 28:2477–2491. [PubMed: 25344324]
12. Martinez P, et al. Increased telomere fragility and fusions resulting from TRF1 deficiency lead to degenerative pathologies and increased cancer in mice. Genes Dev. 2009; 23:2060–75. [PubMed: 19679647]
13. Denchi EL, de Lange T. Protection of telomeres through independent control of ATM and ATR by TRF2 and POT1. Nature. 2007; 448:1068–71. [PubMed: 17687332]
14. Griffith JD, et al. Mammalian telomeres end in a large duplex loop. Cell. 1999; 97:503–514. [PubMed: 10338214]

Europe PMC Funders Author Manuscripts

15. Doksani Y, Wu JY, de Lange T, Zhuang XW. Super-Resolution Fluorescence Imaging of Telomeres Reveals TRF2-Dependent T-loop Formation. Cell. 2013; 155:345–356. [PubMed: 24120135]
16. Amiard S, et al. A topological mechanism for TRF2-enhanced strand invasion. Nat Struct Mol Biol. 2007; 14:147–154. [PubMed: 17220898]
17. Benarroch-Popivker D, et al. TRF2-Mediated Control of Telomere DNA Topology as a Mechanism for Chromosome-End Protection. Mol Cell. 2016; 61:274–86. [PubMed: 26774283]
18. Court R, Chapman L, Fairall L, Rhodes D. How the human telomeric proteins TRF1 and TRF2 recognize telomeric DNA: a view from high-resolution crystal structures. EMBO Rep. 2005; 6:39–45. [PubMed: 15608617]
19. Wu H, Lima WF, Crooke ST. Investigating the structure of human RNase H1 by site-directed mutagenesis. J Biol Chem. 2001; 276:23547–53. [PubMed: 11319219]
20. Deng Z, Norseen J, Wiedmer A, Riethman H, Lieberman PM. TERRA RNA binding to TRF2 facilitates heterochromatin formation and ORC recruitment at telomeres. Mol Cell. 2009; 35:403–13. [PubMed: 19716786]
21. Apte MS, Cooper JP. Life and cancer without telomerase: ALT and other strategies for making sure ends (don't) meet. Crit Rev Biochem Mol Biol. 2017; 52:57–73. [PubMed: 27892716]
22. Arora R, et al. RNaseH1 regulates TERRA-telomeric DNA hybrids and telomere maintenance in ALT tumour cells. Nat Commun. 2014; 5:5220. [PubMed: 25330849]
23. Boguslawski SJ, et al. Characterization of monoclonal antibody to DNA.RNA and its application to immunodetection of hybrids. J Immunol Methods. 1986; 89:123–30. [PubMed: 2422282]
24. Smith S, Giriat I, Schmitt A, de Lange T. Tankyrase, a poly(ADP-ribose) polymerase at human telomeres. Science. 1998; 282:1484–1487. [PubMed: 9822378]
25. Dynek JN, Smith S. Resolution of sister telomere association is required for progression through mitosis. Science. 2004; 304:97–100. [PubMed: 15064417]
26. Nguyen HD, et al. Functions of Replication Protein A as a Sensor of R Loops and a Regulator of RNaseH1. Mol Cell. 2017; 65:832–847 e4. [PubMed: 28257700]
27. Munoz P, Blanco R, Flores JM, Blasco MA. XPF nuclease-dependent telomere loss and increased DNA damage in mice overexpressing TRF2 result in premature aging and cancer. Nat Genet. 2005; 37:1063–71. [PubMed: 16142233]
28. Nera B, Huang HS, Lai T, Xu L. Elevated levels of TRF2 induce telomeric ultrafine anaphase bridges and rapid telomere deletions. Nat Commun. 2015; 6:10132. [PubMed: 26640040]
29. Tong AS, et al. ATM and ATR Signaling Regulate the Recruitment of Human Telomerase to Telomeres. Cell Rep. 2015; 13:1633–1646. [PubMed: 26586433]
30. Balk B, et al. Telomeric RNA-DNA hybrids affect telomere-length dynamics and senescence. Nat Struct Mol Biol. 2013; 20:1199–205. [PubMed: 24013207]
31. Graf M, et al. Telomere Length Determines TERRA and R-Loop Regulation through the Cell Cycle. Cell. 2017; 170:72–85 e14. [PubMed: 28666126]
32. Fouche N, et al. The basic domain of TRF2 directs binding to DNA junctions irrespective of the presence of TTAGGG repeats. J Biol Chem. 2006; 281:37486–95. [PubMed: 17052985]
33. Poulet A, et al. TRF2 promotes, remodels and protects telomeric Holliday junctions. EMBO J. 2009; 28:641–51. [PubMed: 19197240]
34. Schmutz I, Timashev L, Xie W, Patel DJ, de Lange T. TRF2 binds branched DNA to safeguard telomere integrity. Nat Struct Mol Biol. 2017; 24:734–742. [PubMed: 28805810]
35. Santos-Pereira JM, Aguilera A. R loops: new modulators of genome dynamics and function. Nat Rev Genet. 2015; 16:583–97. [PubMed: 26370899]
36. Lee YW, Kim WT. Telomerase-dependent 3' G-strand overhang maintenance facilitates GTBP1-mediated telomere protection from misplaced homologous recombination. Plant Cell. 2013; 25:1329–42. [PubMed: 23572544]

Europe PMC Funders Author Manuscripts

Europe PMC Funders Author Manuscripts

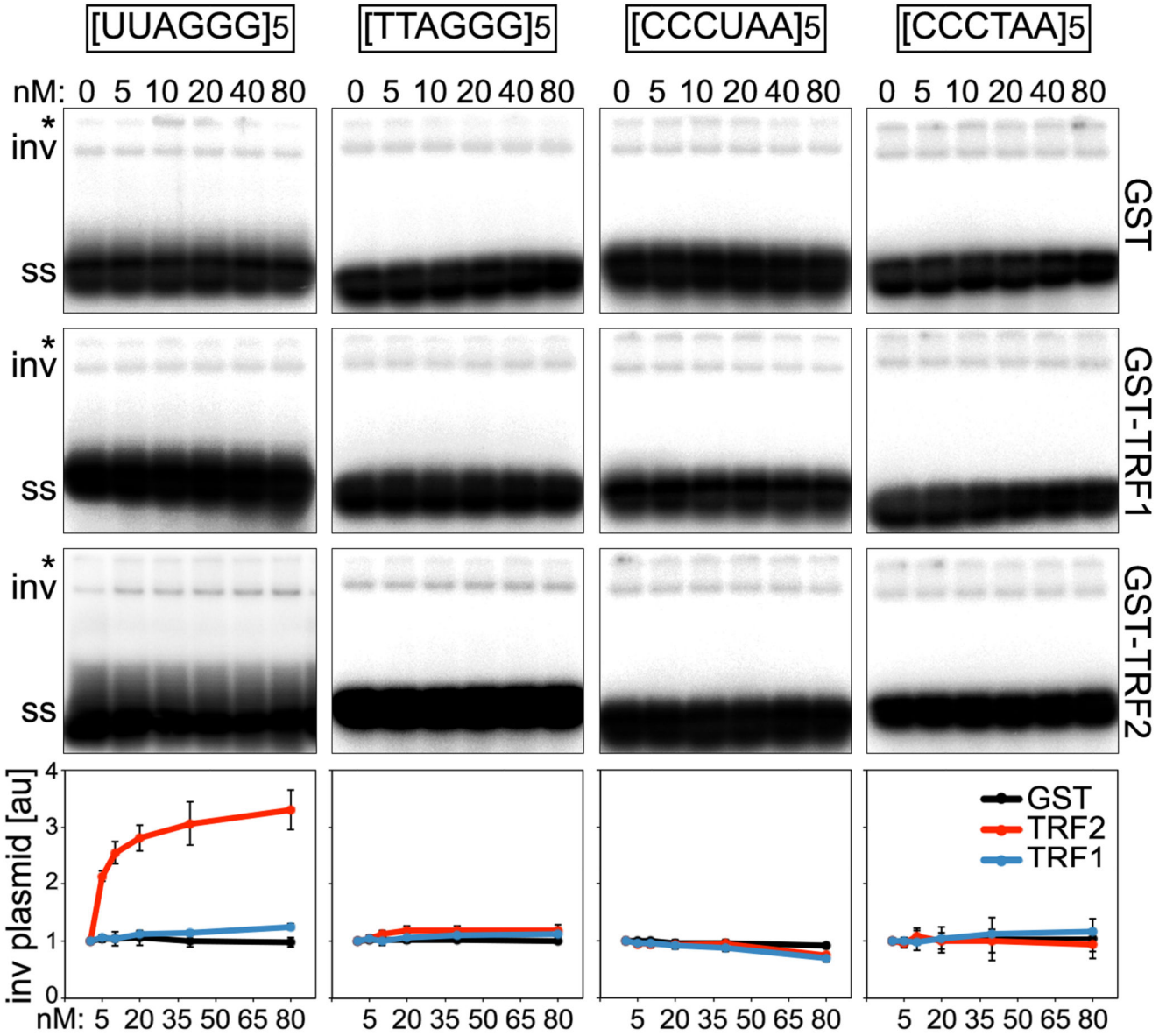

Figure 1. TRF2 promotes TERRA invasion into telomeric dsDNA.

Strand invasion assays with the indicated telomeric RNA or DNA oligonucleotides (10 nM) in combination with p-Tel plasmid (0.6 nM) and increasing amounts of glutathione S-transferase (GST), GST-TRF1 or GST-TRF2. Invaded plasmids (inv) were quantified and graphed as the fold increase compared with samples lacking proteins (bottom). Values are means ± SD (n = 3 independent experiments). ss, single stranded oligonucleotides; *, wells. Uncropped images are shown in **Supplementary Data Set 1**.

Europe PMC Funders Author Manuscripts

Europe PMC Funders Author Manuscripts

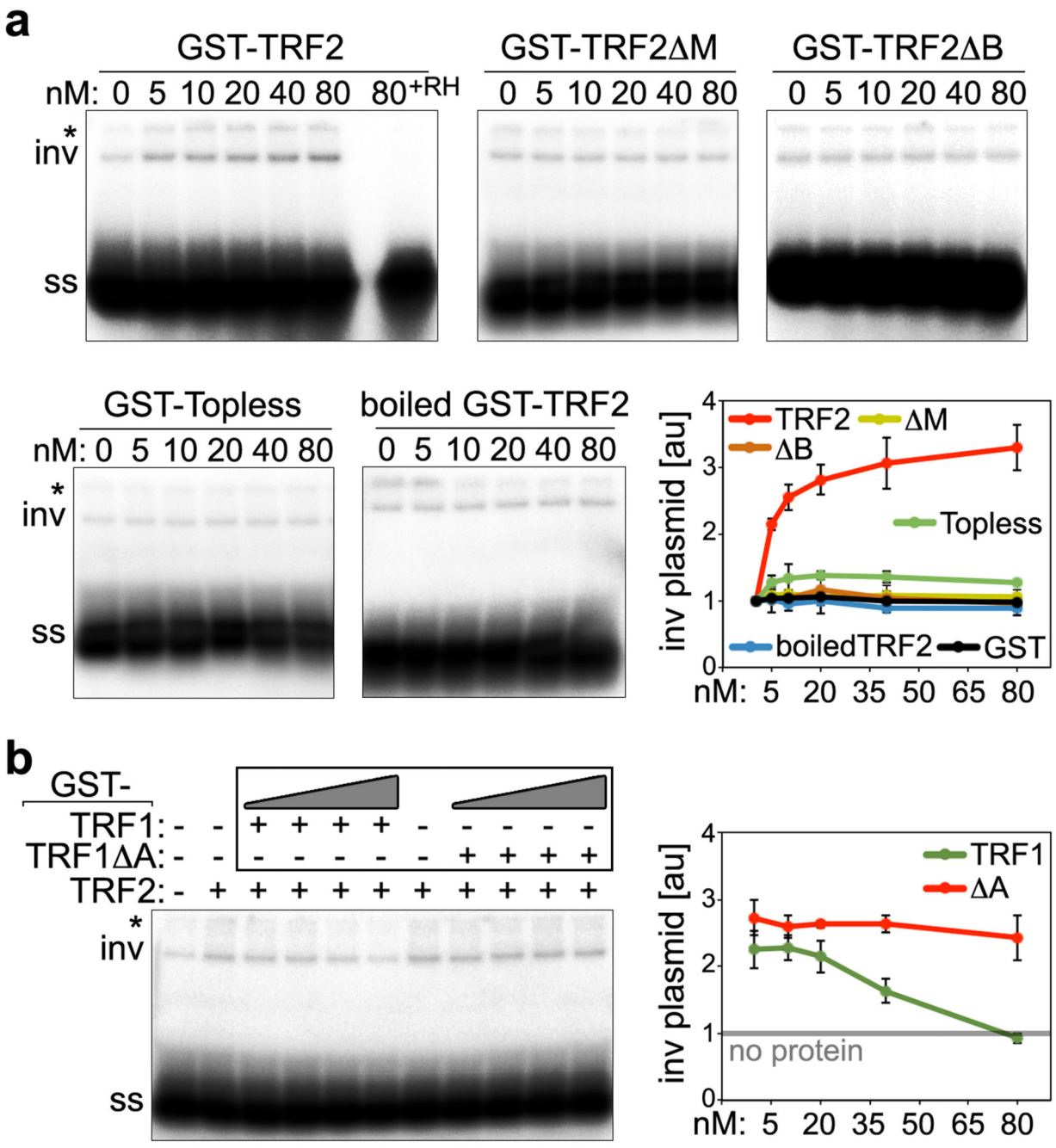

Figure 2. TRF1 A domain suppresses TRF2-stimulated TERRA invasion into telomeric dsDNA.

(**a**) Strand invasion assays with $(UUAGGG)_5$ TERRA-like oligonucleotides (10 nM), p-Tel plasmid (0.6 nM) and increasing amounts of the indicated recombinant proteins. A control assay was performed with heat denatured (boiled) GST-TRF2. (**b**) Invasion assays in presence of 40 nM GST-TRF2 and increasing amounts (0, 10, 20, 40 and 80 nM) of GST-TRF1 or GST-TRF1ΔA. Invaded plasmids (inv) were quantified and graphed as the fold increase compared with samples lacking proteins. Values are means ± SD ($n = 3$ independent experiments). ss, single-stranded RNA oligonucleotide; RH, RNaseH treatment

prior to electrophoresis; *, wells. Uncropped images are shown in **Supplementary Data Set 1**.

Europe PMC Funders Author Manuscripts

Europe PMC Funders Author Manuscripts

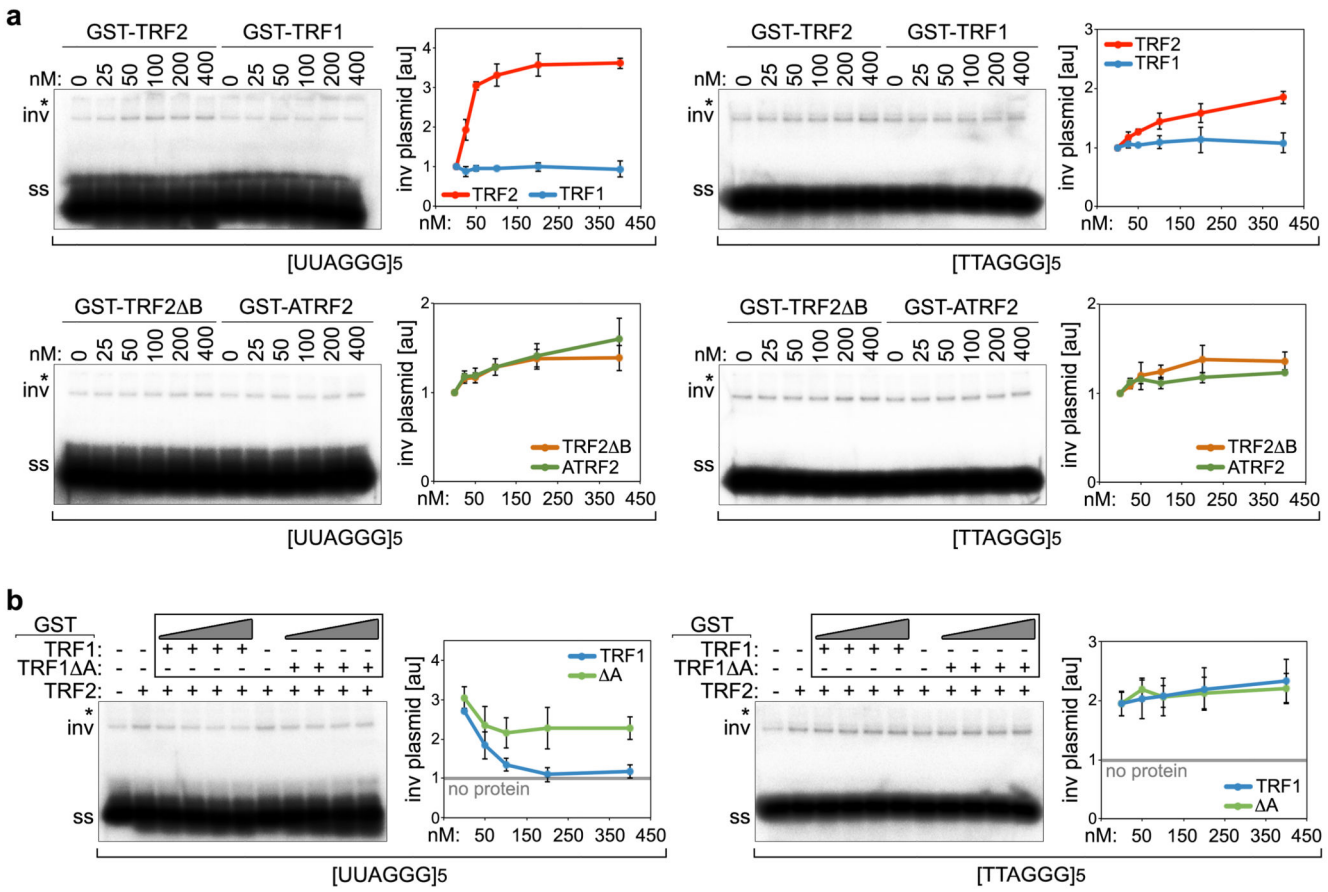

Figure 3. Strand invasion assays with telomeric RNA and DNA oligonucleotides and high concentrations of TRF proteins.

(**a**) Strand invasion assays with G-rich telomeric RNA or DNA oligonucleotides (10 nM), p-Tel plasmid (0.6 nM) and increasing amounts of the indicated recombinant proteins. (**b**) Invasion assays in presence of 200 nM GST-TRF2 and increasing amounts (0, 25, 50, 100, 200 and 400 nM) of GST-TRF1 or GST-TRF1ΔA. Invaded plasmids (inv) were quantified and graphed as the fold increase compared with samples lacking proteins. Values are means ± SD (n = 3 independent experiments). ss, single stranded oligonucleotides; *, wells. Uncropped images are shown in **Supplementary Data Set 1**.

Europe PMC Funders Author Manuscripts
Europe PMC Funders Author Manuscripts

Europe PMC Funders Author Manuscripts

Europe PMC Funders Author Manuscripts

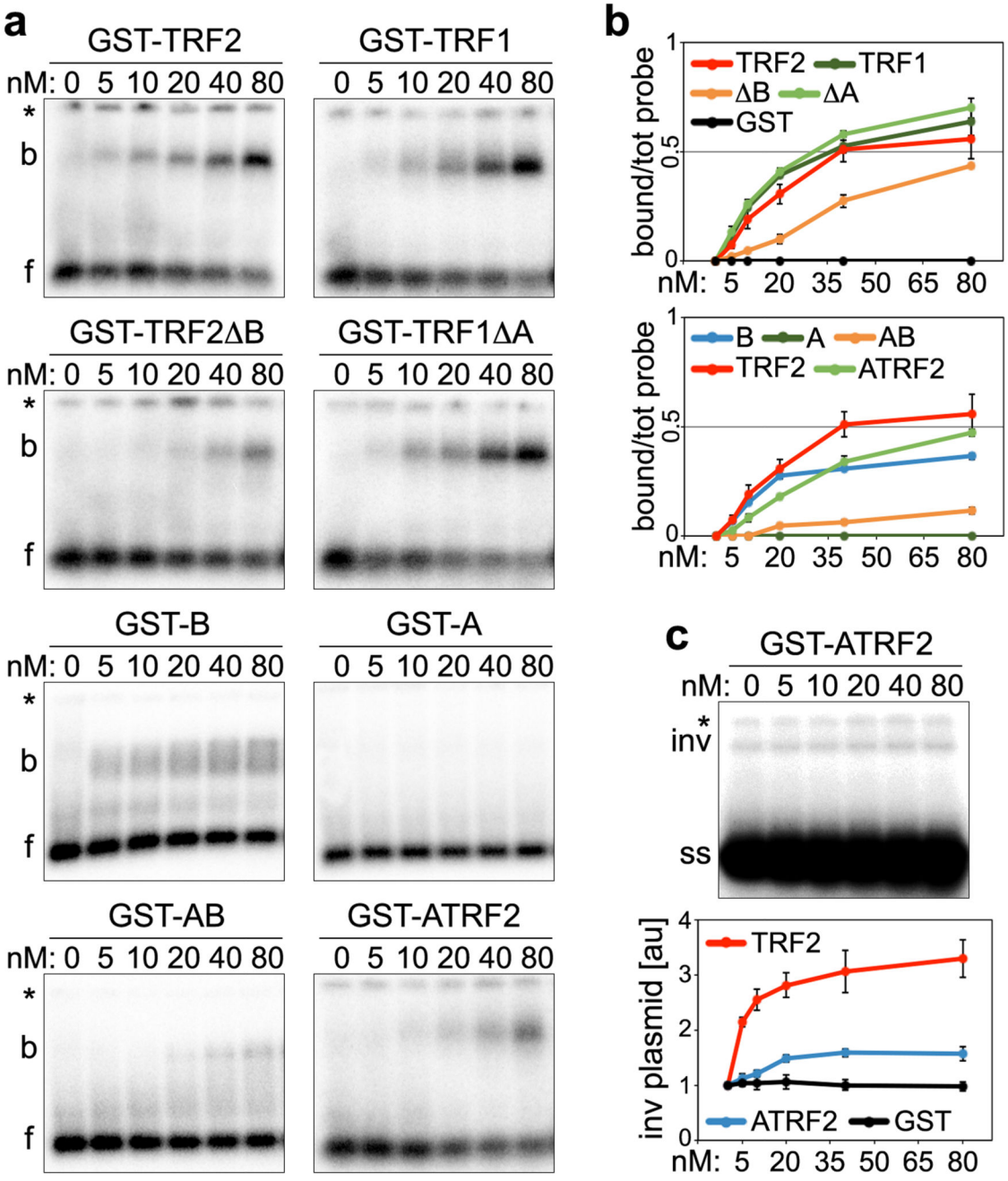

Figure 4. TRF1 A domain suppresses TERRA binding to TRF2 B domain.

(**a**) Electromobility shift assays with $(UUAGGG)_5$ TERRA-like oligonucleotides (0.25 nM) and increasing amounts of the indicated recombinant proteins. f, free probe; b, bound probe; *, wells. (**b**) Bound oligonucleotides were quantified and graphed as fraction of the total signal within each lane. Values are means ± SD (n = 3 independent experiments). (**c**) Strand invasion assay with $(UUAGGG)_5$ TERRA-like oligonucleotides (10 nM), p-Tel plasmid (0.6 nM) and increasing amounts of GST-ATRF2. Invaded plasmids (inv) were quantified and graphed as the fold increase compared with samples lacking proteins. Values are means ±

SD (n = 3 independent experiments). ss, single stranded oligonucleotides; *, wells. Uncropped images are shown in **Supplementary Data Set 1**.

Europe PMC Funders Author Manuscripts

Europe PMC Funders Author Manuscripts

Europe PMC Funders Author Manuscripts

Europe PMC Funders Author Manuscripts

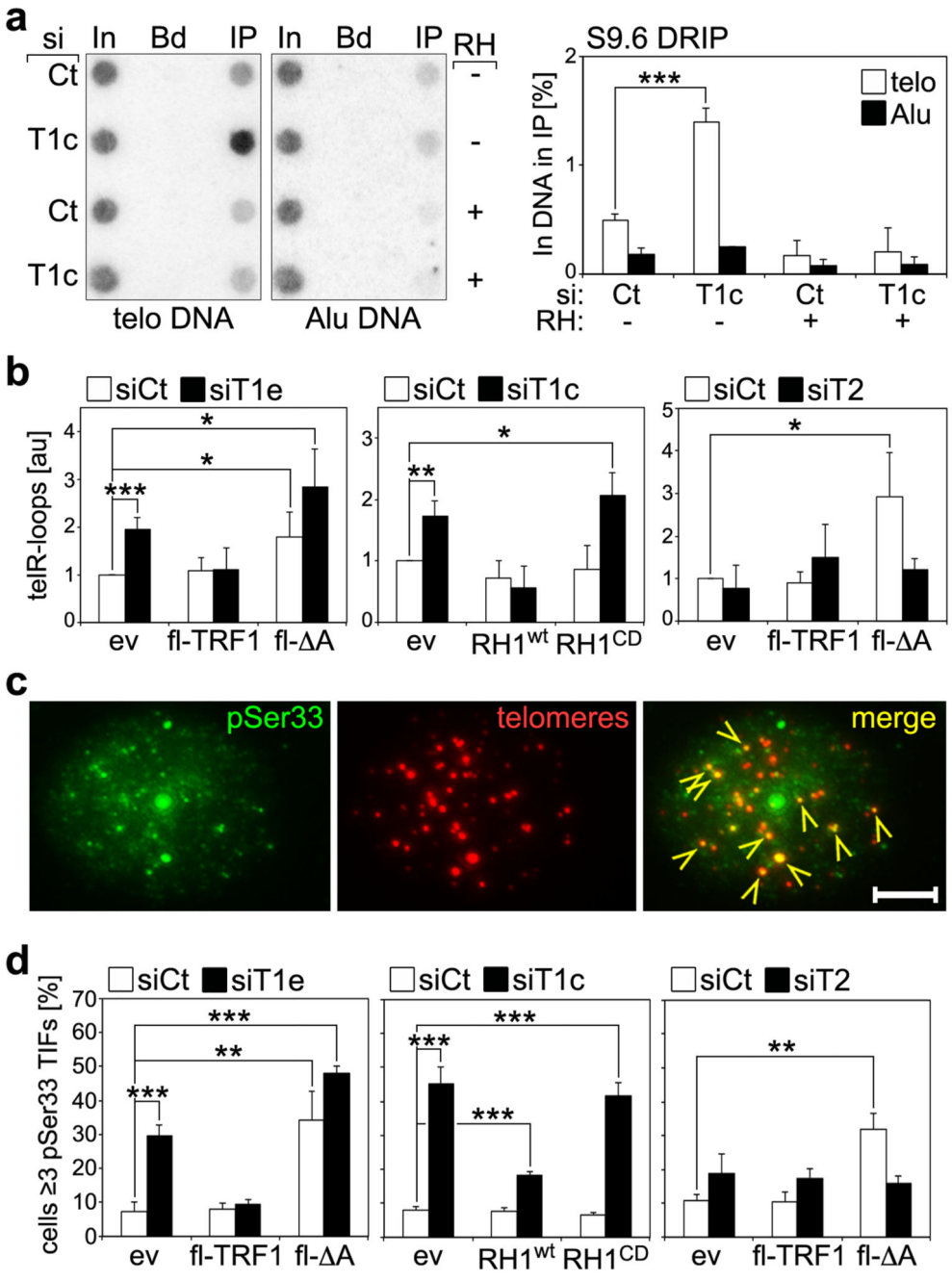

Figure 5. TRF1 A domain suppresses TRF2-mediated accumulation of telR-loops and pSer33 TIFs in HeLa cells.

(**a**) Telomeric and Alu repeat dot-blot hybridization of S9.6 DRIPs of HeLa cells transfected with siRNAs against TRF1 (T1c) or control siRNAs (Ct). Uncropped images are shown in **Supplementary Data Set 1**. Nucleic acids were collected 4 days after transfection. In, input (1%); Bd, beads only control (100%); IP, S9.6 immunoprecipitated material (100%). RH, RNaseH treatment of nucleic acids prior to immunoprecipitation. Signals are graphed as the fraction of In DNA found in IPs after subtraction of Bd-associated signal. Values are means

± SD (n = 3 independent experiments). (**b**) Quantifications of S9.6 DRIP experiments in HeLa cells transfected with siRNAs against TRF1 (siTc or siTe) or TRF2 (siT2) and infected with retroviruses expressing siT1e-insensitive, flag tagged TRF1 (fl-TRF1) and TRFΔA (fl-ΔA), or wild type (wt) and catalytically dead (CD) forms of RNaseH1 (RH1). Nucleic acids were collected 4 days after siRNA transfections and expression of ectopic proteins. Quantifications are of fraction of telomeric In DNA found in IPs after subtraction of Bd-associated signal and normalization over empty vector (ev)-infected, siCt-transfected cells. Values are means ± SD (n = 4 independent experiments for the first two graphs from the left; n = 3 for the graph on the right). (**c**) Example of pSer33 immunostaining (green) combined with telomeric DNA FISH (red) on cells transfected with siT1c. Arrowheads point to pSer33 TIFs. Scale bar, 5 μm. (**d**) Percentages of cells with at least 3 pSer33 TIFs in cells as in **b** graphed as means ± SD (n = 3 independent experiments). *P < 0.05, **P < 0.005, ***P < 0.0001 (two-tailed Student's t-test).

Europe PMC Funders Author Manuscripts

Europe PMC Funders Author Manuscripts

Europe PMC Funders Author Manuscripts

Europe PMC Funders Author Manuscripts

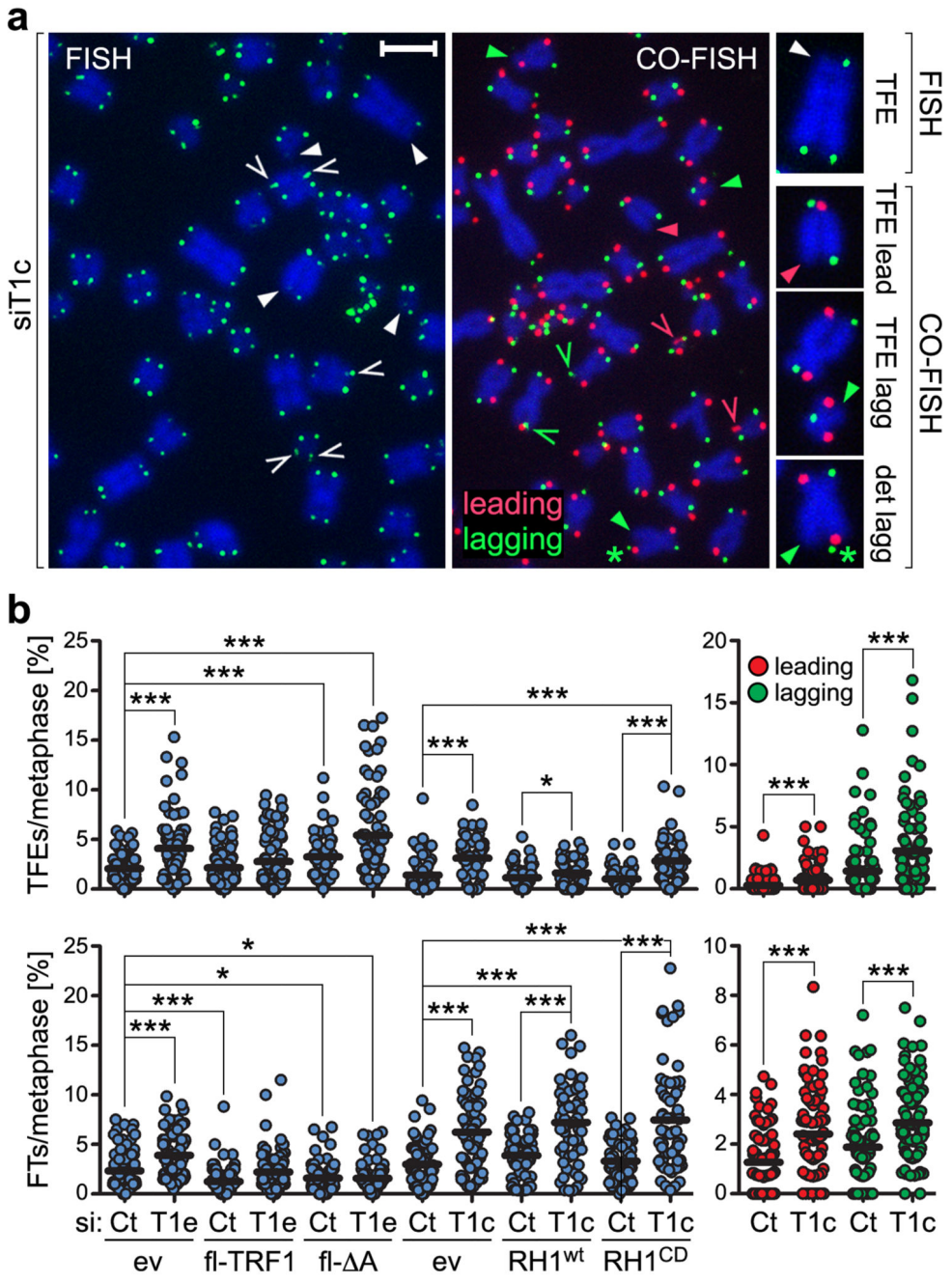

Figure 6. TRF1 A domain suppresses telR-loop-induced telomere loss in HeLa cells.

(**a**) Examples of telomeric DNA FISH and CO-FISH on metaphases from HeLa cells transfected with siT1c. Filled arrowheads point to TFEs, not filled arrowheads to FTs, the asterisk indicates a telomeric fragment. Scale bar, 5 μm. (**b**) Quantifications of TFEs and FTs in FISH and CO-FISH experiments on HeLa cells transfected with siT1c or siT1e and infected with retroviruses expressing fl-TRF1, fl-ΔA, $RH1^{wt}$ or $RH1^{CD}$. Cells were harvested 4 days after siRNA transfection and expression of ectopic proteins. For FISH, at least 4400 chromosomes from 3 independent experiments (except for ev samples, where data

are from 4 independent experiments) were analyzed for each condition. For CO-FISH, at least 3200 chromosomes from three independent experiments were analyzed for each condition. Dots are percentages of FTs or TFEs per chromosome end in one metaphase. Black bars are means. *$P < 0.05$, ***$P < 0.0001$ (Mann-Whitney U test).

Europe PMC Funders Author Manuscripts

Europe PMC Funders Author Manuscripts

Europe PMC Funders Author Manuscripts

Europe PMC Funders Author Manuscripts

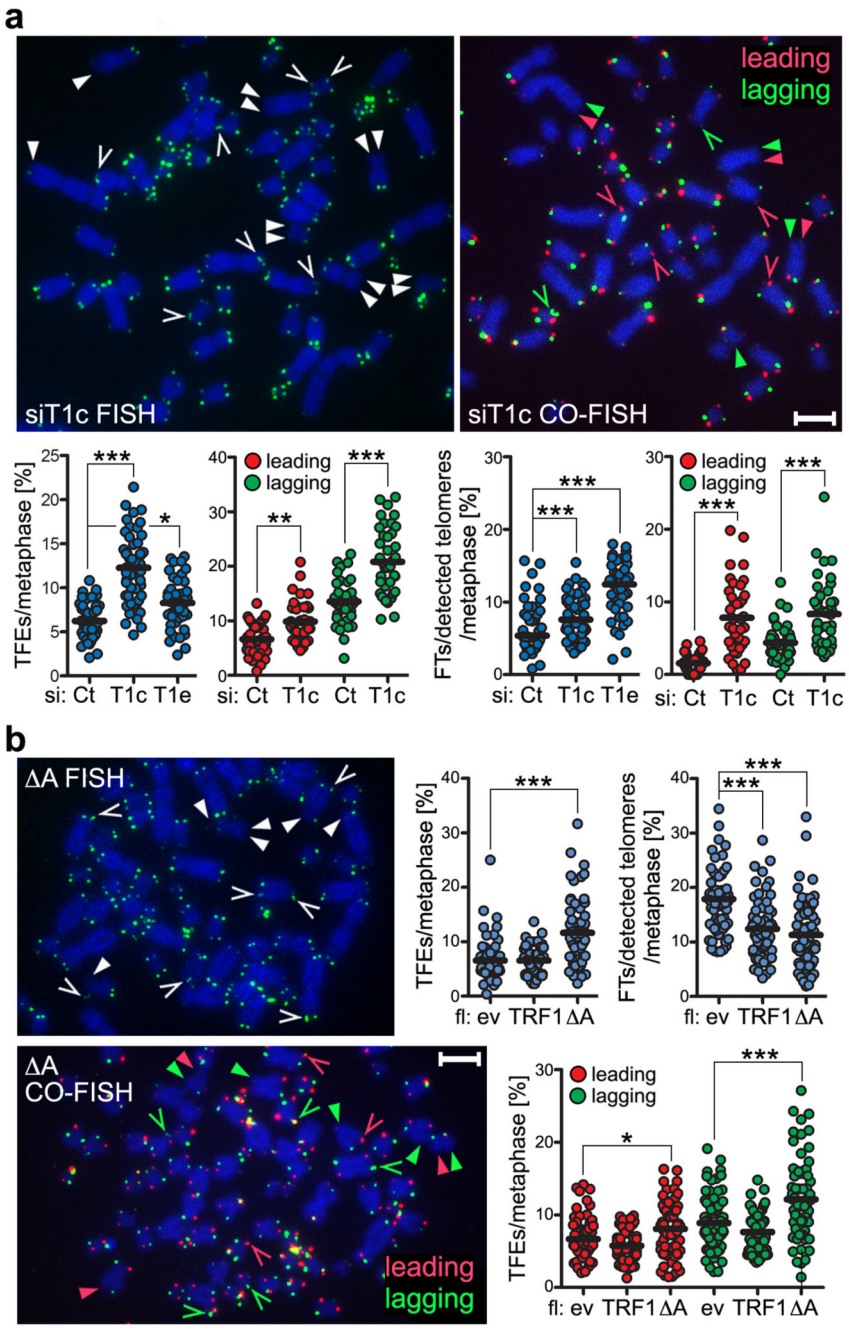

Figure 7. TRF1 A domain suppresses telomere loss in U2OS cells.

(**a**) Examples of telomeric DNA FISH and CO-FISH on metaphases from U2OS cells transfected with siT1c. Cells were harvested 3 days after siRNA transfection. Filled arrowheads point to examples of TFEs, not filled arrowheads point to examples of FTs. Scale bar, 5 μm. Scatter plots are quantifications of TFEs and FTs in FISH and CO-FISH experiments. At least 2700 (for FISH) and 4300 (CO-FISH) chromosomes from 3 independent experiments were analyzed for each condition. siT1c and siT1e are two independent siRNAs against TRF1; siCt: control siRNA. (**b**) Telomeric DNA FISH and CO-

FISH on metaphases from fl-ΔA-expressing U2OS cells. Cells were harvested after 4 days of ectopic protein expression. ev: empty vector retrovirus. Filled arrowheads point to examples of TFEs, not filled arrowheads point to examples FTs. Scale bar, 5 μm. Scatter plots are quantifications of TFEs and FTs in FISH and CO-FISH experiments. At least 4100 (FISH) and 4800 (CO-FISH) chromosomes from 3 independent experiments were analyzed for each condition. For TFEs dots are percentages per chromosome end in one metaphase, while for FTs dots are percentages per chromosome end with detectable telomeric signal in one metaphase due to the large number of TFEs accumulating in the same cells. Black bars are means. *$P < 0.05$, **$P < 0.005$, ***$P < 0.0001$ (Mann-Whitney U test).

Europe PMC Funders Author Manuscripts

Europe PMC Funders Author Manuscripts

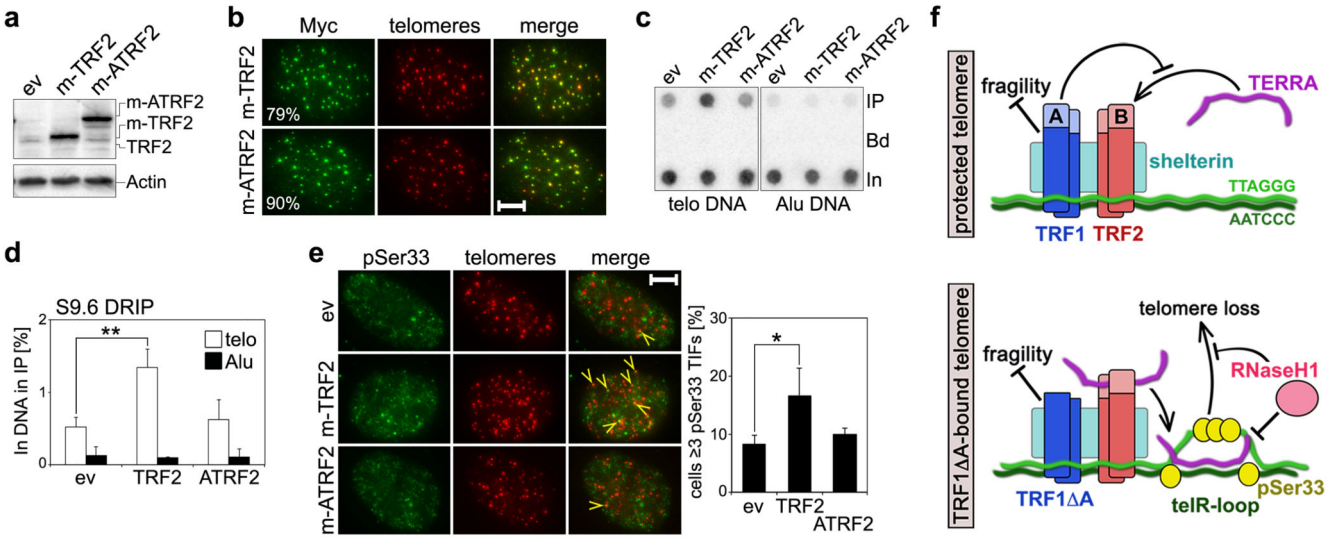

Figure 8. TRF2 over-expression leads to accumulation of telR-loops and pSer33 TIFs in HeLa cells.

(**a**) Western blot analysis of HeLa cells infected with lentiviruses driving expression of myc-tagged TRF2 (m-TRF2) or ATRF2 (m-ATRF2) from a doxycycline inducible promoter, or with empty vector (ev) lentiviruses. Cells were treated with doxycycline for 4 days. The TRF2 antibody detects endogenous TRF2, m-TRF2 and m-ATRF2. Actin serves as a loading control. Uncropped images are shown in **Supplementary Data Set 1**. (**b**) Myc immunostaining (green) combined with telomeric DNA FISH (red) on cells as in **a**. Numbers are percentages of cells expressing the ectopic proteins. Scale bar, 5 μm. (**c**) Telomeric and Alu repeat dot-blot hybridization of S9.6 DRIPs of cells as in **a**. Uncropped images are shown in **Supplementary Data Set 1**. In, input (1%); Bd, beads only control (100%); IP, S9.6 immunoprecipitated material (100%). (**d**) Quantification of experiments as in **c**. Signals are graphed as the fraction of In DNA found in IPs after subtraction of Bd-associated signal. Values are means ± SD ($n = 3$ independent experiments). (**e**) pSer33 immunostaining (green) combined with telomeric DNA FISH (red) on cells as in **a**. Arrowheads point to examples of pSer33 TIFs. Scale bar, 5 μm. Percentages of cells with at least 3 pSer33 TIFs are graphed as means ± SD ($n = 3$ independent experiments). *$P < 0.05$, **$P < 0.005$ (two-tailed Student's t-test). (**f**) Speculative model for TRF1, TRF2 and TERRA interplay at telomeres. At a fully protected chromosome end TRF1 A domain prevents TRF2 B domain from interacting with TERRA. When TRF1 is replaced with TRF1ΔA, TERRA interaction with TRF2 B domain drives TERRA invasion into telomeric dsDNA and formation of telR-loops, which in turn promote pSer33 binding to telomeres and telomere loss. pSer33 might bind to both ss G-rich or C-rich telomeric DNA.

Europe PMC Funders Author Manuscripts
Europe PMC Funders Author Manuscripts